A combined mixing model for high-frequency concentration–discharge relationships

José Manuel Tunqui Neira, Gaëlle Tallec, Vazken Andréassian, Jean-Marie Mouchel

A combined mixing model for high-frequency concentration-discharge relationships

José Manuel Tunqui Neira[1, 2], Gaëlle Tallec[1,*], Vazken Andréassian[1] & Jean-Marie Mouchel[2]
(1) Université Paris-Saclay, INRAE, HYCAR Research Unit, 92761 Antony, France
(2) Sorbonne Université, CNRS, EPHE, UMR METIS 7619, Paris, France
* corresponding author

Highlights

- A new combined mixing model for concentration-discharge relationships.
- A formula combining dynamics of the discharge, with dynamics of the ion concentrations.
- An unusual approach of hydrograph separation.
- How coupling a time dynamic hydrological model with static $C - Q$ relations.

Abstract

Streamflow is the major factor influencing the evolution of solute concentration in river water and different modelling approaches exist to characterize the dependency of ion concentration to discharge: the simplest are based on measurable quantities (stream discharge and stream ion concentration) but do not allow for an explicit, physical, flow-path interpretation; the more complex are based on mixing assumptions with different end-members sources, but require the knowledge of (unmeasurable) flow components. We present here a new concentration-discharge model, which associates a classical concentration-discharge relationship with a classical two-component mixing equation. The originality of our approach lies in the fact that we do not proceed in the usual way to perform the hydrograph separation: we use an *a priori* assumption of the baseflow-quickflow separation to infer the source concentration values, contrarily to the usual (inverse) approach. The other notable originality is that all the parameters of this model depend on the temporal variation of the stream discharge. This combined model was tested on high-frequency ion concentration series from the ORACLE-Orgeval observatory (France). This work demonstrates that high temporal resolution data allows for explicit testing of model performance across different hydrologic scales. Results show that the combined mixing model allows a better estimation of streamflow solute concentration series for most ions tested at inter-annual scale, except for nitrate (which do not exhibit a clear $C - Q$ relationship). Our results also confirm the advantage of coupling a time dynamic hydrological model with static $C - Q$ relations for each of the flow components.

Keywords

Concentration-discharge relationships; high-frequency measurements; mixing equations.

1. Introduction

Concentration-discharge ($C-Q$) relationships are interesting for a variety of purposes and potential users and because they employ simple approaches to describe complex hydro-chemical interactions, hydrologists and geochemists have been using and exploring them for over 70 years (see Chanat et al., 2002; Durum, 1953; Hem, 1948; Johnson et al., 1969; Kirchner, 2019; Moatar et al., 2017). The established relations can be purely empirical, used to infill lacking concentration data and compute fluxes over long time periods, or to characterize the regime export of chemical components in a number of catchments and empirically derive euristic patterns on a regional and global scale (e.g. Bieroza et al., 2018; Meybeck and Moatar, 2012; Moatar et al., 2017). In some cases, the relations have been derived from a more complex model, describing a physical representation of water circulation and composition, from various mixing sources, with the objective to derive relevant information on internal functionning (Johnson et al., 1969).

To model $C-Q$ relationships, two classical approaches exist:

- The temporal $C-Q$ patterns relationship (i.e. fit parameters of C vs Q, Musolff et al. (2017)) try to explain the processes controlling the mobilization and delivery of chemical elements into streams (i.e. export regimes): dilution, flow-enhancement, or no-variation at all (see e.g. Salmon et al., 2001), as well as biogeochemical transformations in river networks (Minaudo et al., 2019). These models are, first and foremost, based on observations of concentrations relatively stable over time, as electro-conductivity (EC) or chlorides (Durum, 1953; Hem, 1948). Often, the main objective is to identify the groundwater contribution to streamflow (Durum, 1953). These models are based on measurable quantities (discharge and in-stream chemical concentrations) (Durum, 1953; Hem, 1948; Tunqui Neira et al., 2020) (see example, Eq. (1) and Eq. (2) in Table 1).
- The more complex *n*-component models have in addition the aim of quantifying the sources of the chemical concentrations measured in the river (Barthold et al., 2011). Introduced at the end of the 1960s (Hubert et al., 1969; Johnson et al., 1969; Pinder and Jones, 1969), they are based on the chemical contribution of hydrological sources (i.e. groundwater, runoff, precipitation), assuming each one can be characterized by a constant concentration and assuming the existence of a methodology to identify the relative contribution of each source to streamflow. This mixing approach is based on the mass balance equation (see its simplest

66 expression, Eq. (3), Table 1). Hall (1970) gives an exhaustive presentation of these models,
67 their different expressions and assumptions. The mixing model was applied at different time
68 scale from flood and event scale (Hubert et al., 1969; Pinder and Jones, 1969) to annual scale
69 (Johnson et al., 1969) and for different purposes such as hydrograph separation (Pinder and
70 Jones, 1969), understanding of flowpaths in catchment (Johnson et al., 1969), or the
71 dynamics of the components of storm flow (Hubert et al., 1969).

72 Table 1: Classical $C - Q$ relationships used in literature

Approach	Equation	Number of parameters	Formula	Eq. n°
Temporal $C - Q$ patterns	Power-law	2	$C = aQ^b$	Eq. (1)
	Two-sided power-law equation	3	$C^{\frac{1}{n}} = a + bQ^{\frac{1}{n}}$	Eq. (2)
Mixing end-member sources	mixing model (*with at least two sources which can be simplified with base flow and quick flow*)	at least 2	$C = C_b \frac{Q_b}{Q} + C_q \frac{Q_q}{Q}$	Eq. (3)

With
- C : *total streamflow ion concentration at time t (mgL^{-1})*
- Q : *total streamflow (m^3s^{-1}) at time t*
- *a, b, n* : *parameters*
- Q_b : *base flow (m^3s^{-1})*
- Q_q : *quick flow (m^3s^{-1}, $Q_q = Q - Q_b$)*
- C_b : *ion concentration of the base flow (mgL^{-1})*
- C_q : *ion concentration of the quick flow (mgL^{-1})*

73

74 Despite their simplicity, the power-law models can yield excellent fits for some ions, explaining up to
75 90 % of the variance of the concentrations. For this reason, they are still widely used today (Barco et
76 al., 2008; Godsey et al., 2009; Moatar and Meybeck, 2007; Probst and Bazerbachi, 1986). However,
77 several authors have criticized the power-law models, underlining that they lump different hydro-
78 chemical processes and dynamics, and do not allow for an explicit physical flow-path interpretation
79 (Moatar et al., 2017; Rose et al., 2018). Godsey et al. (2009) compared different $C - Q$ models, and
80 concluded that it is difficult to find simple generalizable models that accurately represent the typical
81 shape of the $C - Q$ relationship, which are internally consistent, and make plausible assumptions
82 about catchment behavior.

83 The variability of $C - Q$ relationships could be due to a large number of processes, varying in space,
84 time and with the characteristics of the catchment. The exact mechanisms leading to $C - Q$ relations
85 remain an open question. Both natural and anthropogenic factors affect the biogeochemical
86 response of streams, and, while the majority of solutes show identifiable behaviors in individual
87 catchments, only a minority of behaviors can be generalized (Botter et al., 2019). Some recent

studies attempt to differentiate two distinct behaviors: *chemodynamic* and *chemostasic* export. Chemostasic export is defined as relatively small variations in concentrations compared to discharge (Musolff et al., 2015; Thompson et al., 2011). Chemostasis could be associated with constant rate of chemical weathering (Godsey et al., 2009), "a legacy storage" of anthropogenic nutriment which buffer the variability in concentrations (Basu et al., 2010; Clow and Mast, 2010), or with a significant hydraulic residence time compared to weathering kinetics (Ameli et al., 2017; Maher, 2011). Chemostasic export processes could represent the long-term trend of basin chemistry and can therefore be identified as an average of concentrations (Musolff et al., 2015). Chemodynamic patterns are characterized as high variations in concentrations compared to discharge caused by flushing, enrichment behavior, or dilution behavior (Musolff et al., 2015). It can be controlled: (i) by activation of solute sources heterogeneously distributed in space; (ii) by threshold-driven transport of constituents or (iii) high reactivity of constituents (Jones et al., 2017; Musolff et al., 2015; Vaughan et al., 2017; Zhang et al., 2016). We could also note that Zhang et al. (2016) emphasized that temporal patterns $C - Q$ models (including the b parameter of Eq. (1)) may vary over time or with season, and a single *b* coefficient for the entire period of record is over-simplification and potentially misleading. The other difficulty of a generalization is also the difference in behavior and source of the different ions. Beyond the patterns, changes can occur whether due to weathering, meteorological or anthropic processes, affecting one ion more than another (Knapp et al., 2020; Musolff et al., 2017; Rose et al., 2018; Zhi et al., 2019).

To deal with the non-linearity of the $C - Q$ relationship, some authors have proposed to increase the number of hydrological components (e.g. Evans and Davies, 1998; Probst, 1985), make specific catchment calibration (Godsey et al., 2009), consider flow classes, e.g. low and high flows (Meybeck and Moatar, 2012; Moatar et al., 2017) or integrate significant time steps (Kirchner, 2019). To gain insight into the linkages between chemical and hydrologic processes that yield the observed concentration-discharge relationship, research has often focused on only one of the modeling solutions (i.e. on either power-law model or mixing model).

The temporal patterns (dilution, constant, enrichment) or the mass balance (end-members mixing) approaches are operational and widely used to describe $C - Q$ relationships. There are also other compound methods in the literature, based on solute production models (Ibarra et al., 2016; Maher, 2011; Maher and Chamberlain, 2014) or on end-members models (Bao et al., 2017; Bouchez et al., 2017; Zhi et al., 2019). However, none offers a parsimonious and generalized approach as proposed in this paper. To date, no simple conceptual model still allows combining a dynamic of concentrations with a dynamic of water flow. The new model proposed in this paper is trying to solve this problem, by combining the two approaches (i.e., power-law and mixing model). The originality of

our approach is that we do not proceed by assuming an end-member concentration value to perform the baseflow-quickflow separation, but we use instead the inverse approach, an *a priori* assumption of the baseflow-quickflow using a hydrological hydrograph separation method to infer the source concentration values. All the parameters of the model proposed depend on the temporal variation of the stream discharge. Using the high frequency series of concentrations and discharges, observed during two years on the ORACLE-Orgeval observatory (France), we have tested the performances of this new model at different hydrological time scales and on a full range of flow and concentration. The first aim of this paper is to present the model and its validation on one long high-frequency time-series. The second aim is to discuss of its performances with regards to the classical models. Note that this paper is methodological: it does not focus on the different hydro-chemical processes involved in the composition of the stream solutes or on others watershed functioning considerations.

2. The combined mixing model

The combined model tested here associates a $C-Q$ relationship with a two-component mixing equation:

- As $C-Q$ relationship, we use the two-sided affine power scaling relationship (2S-APS), which we recently proposed to fit the $C-Q$ relationship, as a natural extension of the well-known and widely-used power law relationship (see Tunqui Neira et al., 2020);
- As mixing equation, we use the simplest of the existing schemes, i.e. a two-component equation distinguishing “base flow” and “quick flow” (e.g Pinder and Jones, 1969).

To combine the 2S-APS relationship with the two-component mixing equation (see Eq. (2) and Eq. (3), Table 1), we propose to write the concentrations of each of components in Eq. (3) (i.e. C_b and C_q) as a function of total discharge, using the same transformation:

$$C_b = \left(a_b + b_b Q^{\frac{1}{\mathrm{n}}}\right)^{\mathrm{n}}$$

$$C_q = \left(a_q + b_q Q^{\frac{1}{\mathrm{n}}}\right)^{\mathrm{n}}$$

The total discharge (and not the discharge of each of the two hydraulic components) was used to seek simplification, not increasing too much the number of parameters. We will discuss later the value of this simplification. Then, the mixing equation becomes:

$$C = \left(a_b + b_b Q^{\frac{1}{\mathrm{n}}}\right)^{\mathrm{n}} \frac{Q_b}{Q} + \left(a_q + b_q Q^{\frac{1}{\mathrm{n}}}\right)^{\mathrm{n}} \frac{Q_q}{Q} \qquad \text{Eq. (4)}$$

147 The "combining" procedure merges the two most used forms of equations of the hydro-chemical
148 literature (i.e. Eq. (2) and Eq. (3)). The advantage of this new model is to improve the mixing
149 approach by introducing dynamic concentrations for the sources.Depending on the values taken by
150 parameters a and b in Eq. (4), three schematic situations can be identified, briefly described below
151 and illustrated by Figure 1.

152 ### 2.1. Case 1: chemostatic components ($b_b = b_q = 0$)

153 In this case, C_b and C_q are constant and independent of river discharge. Thus, C is only influenced by
154 the discharge components dynamics (Q_b and Q_q) (see Case 1 in Figure 1). The case 1 represents the
155 chemostatic export characterizing a catchment controlled by large legacy stores (see Musolff et al.,
156 2015). It corresponds to the assumption of the classical mixing equation approach, where the C_b and
157 C_q values can assume for example the average of concentrations, measured respectively during the
158 dry and wet seasons (i.e. Saraiva Okello et al., 2018; Stewart et al., 2007; Zhang et al., 2013).

159 ### 2.2. Case 2: single 2S-APS relationship ($a_b = a_q = a$ and $b_b = b_q = b$)

160 This case reduces to $C_b = C_q$ (Case 2 in Figure 1) and to the simple $C - Q$ relationship:

161 $$C = \left(a + bQ^{\frac{1}{n}}\right)^n$$

162 The observed concentration is only a function of discharge.

163 ### 2.3. Case 3: General case (a and b are different)

164 This is the general case of the transformed mixing equation (Eq. (4)). Unlike the classical mixing
165 equation (chemostatic components), the C_b and C_q values are not constant but vary individually as a
166 function of stream flow (see Case 3 in Figure 1). The general case allows accounting for the temporal
167 variation of the chemical components. It allows connecting concentration with total discharge and
168 the hydrograph separation components (Q_b and Q_q, i.e. with $Q_q = Q - Q_b$, see Table 1).

169

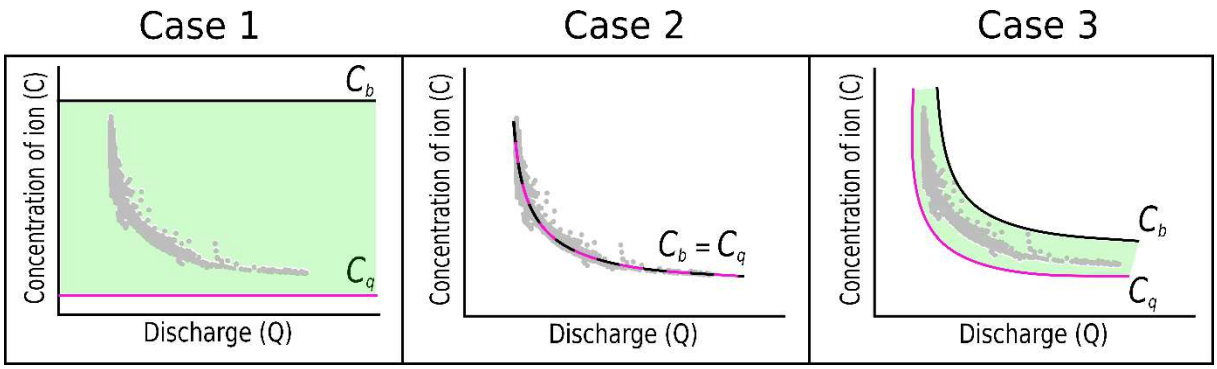

Figure 1: The three hypothetical $C - Q$ scenarios due to the values taken by parameters a and b of Eq. (4): case 1, case 2 and case 3. The green hatching represents the probable C_{sim} yields by our model in the $C - Q$ space.

3. Material and methods

3.1. Study site and datasets

The combined model (Eq. (4)) was applied to the high-frequency hydro-chemical dataset measured at the Oracle-Orgeval Observatory (Tallec et al., 2015) by the *River Lab* (Floury et al., 2017). The Oracle-Orgeval Observatory is a small catchment located 70 km east of Paris, France. It is subjected to a temperate and oceanic climate, with annual average temperature of 11 ± 1 °C and a mean annual rainfall of 674 ± 31 mm (Tallec et al., 2013). The average measured streamflow at the Avenelles outlet (sub-catchment of 46 km^2 and location of the *River Lab* on the Oracle-Orgeval Observatory) is about 0.2 m^3/s (1962 - 2017), with minimum flows in summer (< 0.1 m^3/s) and floods up to 10 m^3/s in winter and spring. With respect to geology, the catchment is underlain entirely by limestone rocks, with two aquifers: the shallower aquifer of the Brie limestone and the deeper Champigny limestone aquifer (Mouhri et al., 2013). Land use is mostly agricultural with few villages, and with intensive farming practices, mainly based on mineral nitrogen fertilization (Garnier et al., 2016). Nearly 60% of the surface of the catchment is drained with tile drains.

Among all ions measured every 30 minutes by the *River Lab* laboratory, we used 3 ions (see Table 2) whose behavior exhibit notable differences in the Orgeval catchment: sulfate, nitrate and chloride. Chloride mainly come from rain inputs during the wet season and to a smaller extent from fertilizers (Floury et al., 2018). Sulfate comes from the chemical weathering of gypsum, which makes it highly variable, depending on the season and the leaching of concerned localized underground layers (Floury et al., 2018; Mouchel et al., 2016). Nitrate mostly come from agricultural activities and fertilizers inputs, with specific seasonal leaching rates (Garnier et al., 2016). Finally, we also used electro-conductivity reflecting the presence of all ions in stream water (EC, see Table 2). The main data set (flow rates and chemical concentrations) covers the period between June 2015 and March 2018 (Table 2), i.e. 20,700 measurements over 33 months. To perform a split-sample test, according

to Klemeš (1986), we divided the dataset into two periods. Table 2 presents a first period used for the model calibration and a second period for the model validation.

Table 2: High-frequency measurements of chemical concentrations (average, minimum, maximum values and difference between quantiles 90 and 10 divided by the mean (CV)) from the *River Lab* at the Avenelles outlet, Oracle-Orgeval Observatory (June 2015 to July 2017 for calibration period and August 2017 to March 2018 for validation period).

Solute	Unit	Calibration period (June 2015 to July 2017)			
		Mean	Min	Max	CV
Sodium	$mg.L^{-1}$	13	2	17	0.12
Sulfate	$mgS.L^{-1}$	19	2	32	0.19
Chloride	$mg.L^{-1}$	30	4	40	0.15
EC	$\mu S.cm^{-1}$	704	267	1015	0.11
		Validation period (August 2017 to March 2018)			
Sodium	$mg.L^{-1}$	13	3	17	0.24
Sulfate	$mgS.L^{-1}$	18	3	26	0.27
Chloride	$mg.L^{-1}$	29	4	40	0.29
EC	$\mu S.cm^{-1}$	576	171	813	0.25

3.2. Hydrograph separation

To apply the combined mixing model (Eq. (4)), we have to separate the hydrograph in order to compute the values of base flow (Q_b) and quick flow (Q_q). To perform the baseflow-quickflow separation (because we do not know the source concentration values) we use an *a priori* assumption of the baseflow-quickflow separation to infer the source concentration values (and not the usual inverse approach).

In this study, we use the Recursive Digital Filter (RDF) hydrograph separation approach. The RDF approach, adapted in the late 1970s from the signal-processing theory, is widely applied for hydrograph separation. Indeed, RDF methods are computationally efficient, easily automated and applied to long continuous streamflow records (Chapman, 1991; Eckhardt, 2005). Among all the RDF-methods existing in literature (Brodie et al., 2007 p.62), we used the well-known Lyne-Hollick method (LH-RDF method) (Lyne and Hollick, 1979; Nathan and McMahon, 1990). Base flow is considered here as a low-frequency signal, and surface runoff as a high-frequency signal. By filtering out the high-frequency signal, the low-frequency signal (i.e. base flow) can be revealed (Longobardi and Loon, 2018; Nathan and McMahon, 1990).

The LH-RDF method is defined as follows:

$$Q_{b(t+1)} = \min\left(\alpha_\tau \, Q_{b(t)} + \frac{1-\alpha_\tau}{2}\left(Q_{(t+1)} + Q_{(t)}\right), Q_{(t)}\right) \quad \text{Eq. (5)}$$

where Q_b, Q, α_τ and t are respectively, the baseflow, the total flow, the LH-RDF filter parameter and the time.

Iterative application of the filter allows smoothing data and nullifying phase distortion. We have used the forward-backward-forward application proposed by Nathan and McMahon (1990). The LH-RDF method is characterized by one parameter (α_τ) which defines the speed of convergence of the filter. It is a common practice (e.g. Longobardi et al., 2016; Zhang et al., 2017) to adapt the filter parameter (α_τ) to the hydrological recession time constant of the catchment (τ). Otherwise, either Q_b or Q_q would have an unwanted behavior on a seasonal time scale (too slow convergence of Q_b or too fast decrease of Q_q during flood events). Another important reason for this adaptation, is that the default value of α_τ (0.925, proposed by Nathan and McMahon, 1990) applied in small catchments controlled by the regional scale factors such as slope and shape, has shown poor performance when computing Q_b (Ladson et al., 2013; Zhang et al., 2017).

During seasons without significant recharge, stream flow may recess exponentially and follows the form:

$$\mathrm{Q}_{(t+\Delta\, t)} = Q_{(t)}.\exp^{(-\frac{\Delta \mathrm{t}}{\tau})} = Q_{(t)}.K \qquad \text{Eq. (6)}$$

where K is the so-called recession constant of the catchment.

The recession constant K can be obtained using the master recession curve (MRC) approach (Nathan and McMahon, 1990). A linear regression (i.e. plot Q_{t+1} vs Q_t see Figure 2A) allows establishing the recession constant *K*, which also represents the α_τ parameter of LH-RDF method (Eq. (5)). This analysis was applied on daily flow data of the Avenelles station from January 1, 2000 to September, 2018 as follows: the daily stream flow data of several seasons were overlapped according to the day of the year, starting from the beginning of June, and assuming that the stream flow decreases under a continuous recession process for the period June-September. The K value obtained about 0.90 has been calculated for a daily discharge (see Figure 2A). However, for high frequency discharge measurements (i.e. time step of 30 min or 0.5 hours), this value must be transformed at the appropriate time step as proposed by Eckhardt (2008) :

$$K_{0.5h} = \left(K_j\right)^{0.5/24} = 0.99$$

With the LH-RDF method (i.e., Eq. (5)) and the calibrated value of K (i.e. 0.99 for the Avenelles catchment), we computed the values of the base flow (Q_b) and the quick flow (Q_q) (see example of the results Figure 2B).

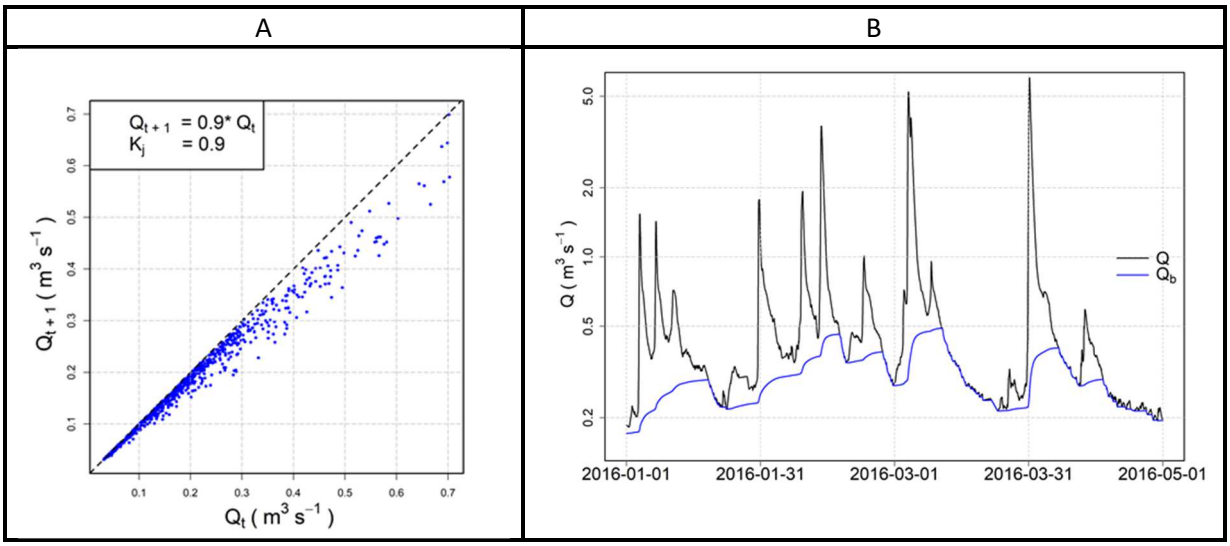

Figure 2: A. Scatter plot of daily discharge Q_{t+1} against Q_t during recession periods, Avenelles station. Dashed black line: line through origin with slope K_j = 0.90. B. Example of hydrograph separation obtained with the LH-RDF method and the constant recession value $K_{0.5h}$ (i.e., 0.99), Avenelles station, with blue line as the baseflow and black line the total flow.

We should not fail to mention here that the baseflow-quickflow methods have been widely criticized: see e.g. Beven (1991) for a vibrant indictment against them and the arguments raised by Pelletier and Andréassian (2019) in the discussion of their paper, for a careful use of them. We do not wish to enter this debate. We will not claim to have identified a precise physical pathway and in this paper, we will thus limit our ambition to the identification of what Pelletier and Andréassian (2020) have named the "*not-too-delayed"* and the "*delayed-enough"* flow components (baseflow and quickflow).

3.3. Calibration of n, a and b parameters

The combined mixing model (Eq. (4)) was applied with the baseflow calculated by the LH-RDF method. For each ion and the EC, we used the parameter n previously determined by Tunqui Neira et al. (2020) on the same data set, but without flow separation.

The extremely large number of values in this high-frequency dataset may cause problems for a robust identification of (a, b) parameters, over the full range of discharges using a simple linear regression. Indeed, the largest discharge values are in small numbers (in our dataset only 1% of discharge values are in the range [2.6 m^3s^{-1}, 12.2 m^3s^{-1}], and they correspond to the lowest concentrations). To address this question, we successively tested a large number of (a,b) pairs from Eq. (4) (n remaining fixed). Each pair yields a series of simulated concentrations (C_{sim}) that can be compared with the observed concentrations (C_{obs}).

Among the many numerical criteria that could be used, we chose the bounded version of the Nash and Sutcliffe (1970) efficiency criterion $NSEB$ (Mathevet et al., 2006), which is commonly used in hydrological modeling. $NSEB$ can be computed on concentrations or on discharge-weighted

concentrations (which corresponds to the load). We chose the average of both, because we found that it allows more weight to be given to the lowest concentrations and thus to avoid the issue of under-representation of high-discharge/low-concentration measurement points. If other criteria exists to test the model performances, the $NSEB_{comb}$ has the advantage to privilege neither the load nor the concentration and integrates both in a single criterion. Table 3 presents the formula for these numerical criteria. We retained as optimal the pair of (a,b) that yielded the highest $NSEB_{comb}$ value (we explored in a systematic fashion the range [1–5] for a and [-1.2–1.2] for b).

Table 3: Numerical criteria used for optimization (C_{obs} – observed concentration, C_{sim} – simulated concentration, Q – observed discharge). The Nash and Sutcliffe (1970) efficiency (NSE) criterion is well known and widely used in the field of hydrology. The rescaling proposed by Mathevet et al. (2006) transforms NSE into NSEB, which varies between -1 and 1 (its optimal value). The advantage of this rescaled version is to avoid the occurrence of large negative values (the original NSE criterion varies in the range [-∞, 1]).

$NSE_{conc} = 1 - \frac{\sum_t (C_{obs}^t - C_{sim}^t)^2}{\sum_t (C_{obs}^t - \overline{C_{obs}})^2}$	Eq. (7)
$NSEB_{conc} = \frac{NSE_{conc}}{2 - NSE_{conc}}$	Eq. (8)
$NSE_{load} = 1 - \frac{\sum_t (Q^t C_{obs}^t - Q^t C_{sim}^t)^2}{\sum_t (Q^t C_{obs}^t - \overline{QC_{obs}})^2}$	Eq. (9)
$NSEB_{load} = \frac{NSE_{load}}{2 - NSE_{load}}$	Eq. (10)
$NSEB_{comb} = \frac{1}{2}(NSEB_{conc} + NSEB_{load})$	Eq. (11)

For each ion and for EC, Table 4 presents the results obtained for the n, a and b parameters calibrated for the Avenelles sub-catchment and their corresponding optimal $NSEB_{comb}$ criterion. Although the parameters of the combined mixing model are shown here, we will not discuss them in this paper. Indeed, for now, without generalized studies covering several catchments it is not possible to interpret them physically. Note that for these reasons we have chosen to present Table 4 in this section and not in the Results and discussion section.

Table 4: Values set for $\boldsymbol{n}$ in the combined model and ($\boldsymbol{a_b}$,$\boldsymbol{b_b}$) and ($\boldsymbol{a_q}$,$\boldsymbol{b_q}$) parameters for each case and solute. Values obtained for optimal $NSEB_{comb}$ criterion. Note that case 1 corresponds to chemostatic components, case 2 to the single 2S-APS relationship and case 3 to general case of the combined model. $NSEB_{comb}$ is optimum in 1.

Solute	*n*	Case	a_b	b_b	a_q	b_q	$NSEB_{comb}$
Sulfate	5	1	1.9	0	1.3	0	0.46
		2	2.2	-0.55	2.2	-0.55	0.69
		3	2.3	-0.7	2	-0.4	0.73
Nitrate	5	1	1.8	0	1.6	0	0.39
		2	1.8	-0.1	1.8	-0.1	0.41
		3	2.3	-1.2	2.1	-0.3	0.45
Chloride	3	1	3.3	0	1.6	0	0.52
		2	3.7	-1	3.7	-1	0.83
		3	3.6	-0.7	3.3	-0.8	0.86
EC	5	1	3.8	0	3.1	0	0.61
		2	4.2	-0.7	4.2	-0.7	0.77
		3	4.2	-0.7	3.9	-0.5	0.83

3.4. Performances of the model

We evaluate the combined model performance in calibration and validation mode. Due to the temporal density of the dataset, we have tested the performances of the models in calibration mode on widely different discharge ranges: over the entire calibration period and for selected storm events (from June 2015 to July 2017, see Table 2, Chapter 3.1). In validation mode, the performances have only been assessed over the entire period (from August 2017 to March 2018, see Table 2, Chapter 3.1).

The $bias$ and the standardized root mean square error ($sRMSE$) allow assessing respectively accuracy and precision of the combined mixing model. Table 5 presents the formula for these numerical criteria.

Table 5: Numerical criteria used for model performance comparison (C_{obs} – observed concentration, C_{sim} – simulated concentration, t – the time step, N – the number of observed concentration)

$bias\ (\%) = 100 * \frac{\sum_t (C_{sim}^t - C_{obs}^t)}{\sum_t (C_{obs}^t)}$	Eq. (13)
$sRMSE\ (\%) = 100 * \frac{\sqrt{\frac{1}{N}\sum_t (C_{obs}^t - C_{cal}^t)^2}}{\overline{C_{obs}}}$	Eq. (14)

4. Results and discussion

4.1. Performance of the combined model over the entire period

Table 6 presents the evaluation of the combined mixing model, in calibration and validation mode over the entire period. Whatever the mode (calibration or validation) and whatever the solute species considered, the optimal $sRMSE$ and $bias$ values are obtained for the general case (Case 3, see Table 6). The results also show that a single 2S-APS relationship (Case 2) explains better the variations of the stream water concentrations than a mass balance equation with constant concentration components (Case 1) (see $sRMSE$ and $bias$ values from case 1 to case 2, Table 6).

Table 6: Values obtained for the $bias$ and the standardized *RMSE* ($sRMSE$) for each case and solute, for an application of the combined model over the entire period. Note that case 1 corresponds to chemostatic components, case 2 to the single 2S-APS relationship and case 3 to general case of the combined model.

Solute	Case	Calibration mode		Validation mode	
		$sRMSE$ %	$bias$ %	$sRMSE$ %	$bias$ %
Sulfate	1	18.3	7.3	24.1	11.7
	2	11.5	3.8	14.8	-11.9
	3	11.3	0.4	10.0	-6.7
Nitrate	1	48.9	46.7	317	315
	2	31.8	30.4	267	266
	3	27.6	-11.2	144	119
Chloride	1	13.8	-4.5	20.0	-0.7
	2	6.3	-0.7	12.6	-3.3
	3	5.3	-0.3	12.1	-0.5
EC	1	10.3	1.5	16.8	7.9
	2	6.0	2.4	9.7	0.5
	3	5.2	-0.5	9.6	-2.7

This means that - within the adopted modelling framework and in as much as the hydrograph separation can be considered as hydrologically relevant - the concentrations of the flow components cannot be considered constant across time (i.e., the behavior of the Avenelles catchment is non-chemostatic). The stream water quality of the Avenelles sub-catchment appears strongly influenced by discharge processes.

The most evident improvement of the case 3 model is observed for chloride and EC (see $sRMSE$ of 5 % with a negative $bias$ less than 0.5% in calibration mode, Table 6). Less importantly, sulfate $sRMSE$ is also much improved when variable concentrations are introduced in the quick and slow components (see $sRMSE$ around 10%, Case 3, in calibration and validation mode Table 6). In calibration mode, the sulfate $bias$ is comparable to that obtained for chloride and EC (less than 0.5%, see Table 6).

According to Floury et al. (2018), chloride would come from the Brie aquifer with mainly external input from rainfall during the wet season. According to Mouchel et al. (2016), the variability of sulfate concentrations is related to the spatial heterogeneity of gypsum lenses and to the temporary variability of the water table heights. The spatial and temporal variability of sulfate and chloride concentrations is due to several chemo-dynamical processes, well modeled by the general case (case 3).

The lowest values of the general case are obtained for nitrate (see $sRMSE$ about 27.6% and a $bias$ about -11.2%, case 3, in calibration mode, and both > 100 % in validation mode, Table 6). Nitrate present the largest seasonal variability, strongly related to farming practices (Garnier et al., 2016) and chemo-dynamic processes especially in the hyporheic-zone (Floury et al., 2018). This larger variability, either environmental or anthropogenic, cannot be simulated by our model, whatever the case.

Figure 3 illustrates the simulations of the models, in the first period of calibration, in regard with the observed time series. As theoretically expected (see Figure 1), the simulated concentrations are more or less dispersed, from linear case 2 to very dispersed case 1 (see Figure 3). The case 3, as shown previously by the $sRMSE$ and the $bias$ (see Table 6), is the one closest to the observed concentrations. For the nitrate, while cases 1 and 2 seem to overestimate the concentrations, case 3 has the advantage, despite its poor performance, of covering all the nitrate concentration values.

A significant feature, common to almost all ions (except nitrate and sulfate) and cases of the model, is the lower C_q concentration, compared to C_b (see black lines *vs* pink lines, Figure 3). For the nitrate ion, C_q concentration becomes a more important contributor in the three cases, until becoming preponderant in the case 3 (see nitrate, pink line Figure 3). For sulfate, C_q is the main contributor to the stream concentration for discharges greater than ~ 0.5 $m^3.s^{-1}$ (see sulfate, pink lines Figure 3).

This result confirm studies carried out at the Orgeval-ORACLE observatory (Billy et al., 2013; Floury et al., 2018; Garnier et al., 2016; Mouchel et al., 2016; Mouhri et al., 2013). Indeed, according to the results, the principal contributor to the stream concentration in the Avenelles catchment would be first groundwater (i.e. C_b) for chloride and EC. During the wet season (i.e. for the discharge beyond 0.5 $m^3.s^{-1}$) for the sulfate and whatever the season for nitrate, the principal contributor is the quickflow concentrations (i.e. C_q). However, the combined mixing model does not seem to be able to consider the quickflow concentrations in a good way; i.e. integrating either the variations of the sub-surface hydrological compartment or the variations of concentrations linked to this compartment.

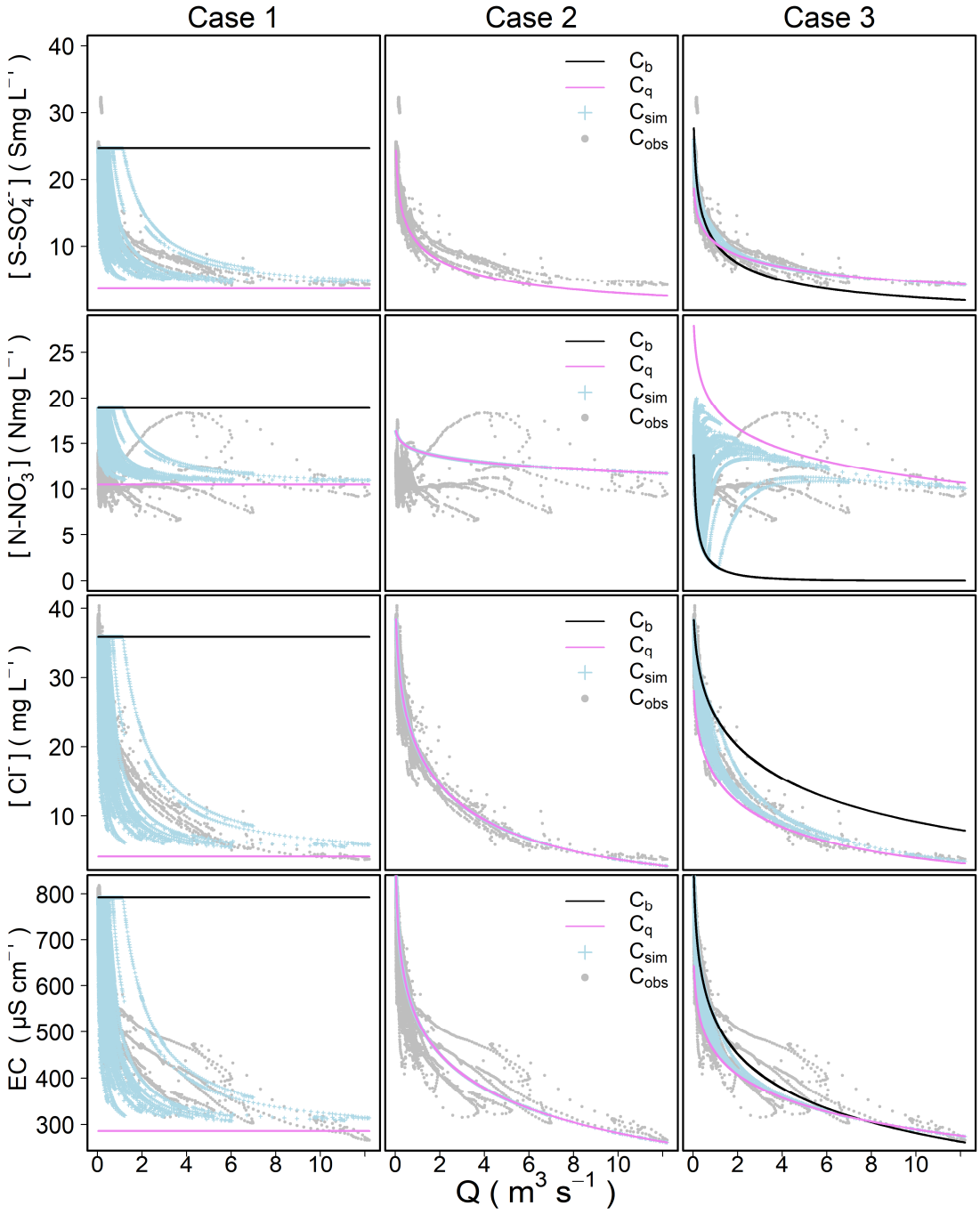

366

367 Figure 3: Simulated concentration (C_{sim}, in blue) obtained of each case of our combined method
368 plotted in the $C - Q$ space for the three ions and EC in the calibration period. In addition, we have
369 plotted the computed values for C_b (black line) and C_q (pink line) for each case studied. Note that in
370 case 2 the lines of C_b and C_q overlap each other. Grey points represent the observed concentrations.

371 ## 4.2. Performances of the combined model for selected storm events

372 We selected two representative flood events of short duration, at the end of fall (November 2015,
373 low groundwater level, low soil moisture and no contribution of tile drains, see Figure 4A) and during
374 winter (February 2016, high groundwater level, high soil moisture and tile drains contribution, see
375 Figure 4B). A longer wet season flood event of March 2016, well covered during 15 days by the

concentration data set, is also added (see Figure 4C). Figure 4 presents observed data and the three cases of simulations with the combined mixing model as a function of time for the three events. For the three selected storm events, Table 7 presents the $sRMSE$ and $bias$ values obtained in a calibration mode with the three cases of the combined model.

At the event scale, except for nitrate during the dry season, we obtain the same results than with the entire period: the case 3 shows the optimal $sRMSE$ and $bias$ values for all ions and EC (see $sRMSE$ and $bias$ from case 1 to case 3, Table 7). The potential advantage of the general case of the combined mixing model (case 3) is to decouple rising and decreasing flow periods with changing Q_q/Q and Q_b/Q ratios (see hydrograph separation, Figure 4). The recursive filter is efficient in separating the base flow from the quick flow. It simulates a quick response of the quick flow at the beginning of flood periods, and a progressive increase of the base flow during the second part of flood periods. Accordingly, the two components model improves the simulation of complex concentration changes during flood events.

We notice that the best results are obtained for the longest flood period: the performances of the case 3 are improved for the long event compared to short events (see $sRMSE$ and $bias$ from short event to long event during wet period, Table 7). As shown in Figure 4C, because of the longer duration of the flood, the recursive filter simulates important variations of the Q_q/Q_b ratio during the event: during most of peak flow period, most of the discharge is due to the quick flow component, while the quick flow component turns back to zero after day 10. As expected from the wider range of Q_q/Q_b ratio, the model simulates more difference between concentrations during the rising part of the event than the descending part (Figure 4C).

We also observe that during short events, the simulated concentrations are slightly shifted compared to the observed concentration (see example for EC, Figure 4). This comes from the limit of our hydrograph separation filter in a flood with a longer duration, the bias due to the time lag is less significant and a wider distribution of the Q_q/Q_b ratio, as simulated by the RDF method, is expected (see Figure 4).

During the wet and dry hydrological seasons, almost all ions behavior (except for nitrates) and EC show a dilution pattern with water of lower concentration followed by a step of increasing concentration (see dotted black line C_{obs}, Figure 4). A common pattern with three stages can be observed in most storm events.

During the first stage we observed a slight increase in concentration during the initial increase in the discharge; then, in the second stage, which is generally short in time, the concentrations strongly

decrease while the discharges quickly increase. In the third stage, both concentrations increase again while discharges continue to decrease and once more reach a lower flow and higher concentration (see Figure 4). To discuss the performances obtained for each case of our combined model, we use the stages outlied above.

The first stage would correspond to a pre-event pattern during which the concentrations come mostly from the groundwater pool (Evans and Davies, 1998; Rose et al., 2018). The following stages correspond to the emergence of soil waters and/or runoff mixing in varying proportions during the event (Evans and Davies, 1998; Rose et al., 2018) (see Figure 4). The contribution of these pools (and the dilution that accompanies it) persists for some time after the peak flow, but in increasingly weaker proportions compared with those of the groundwater. Note that in the dry season, for all ions and EC, the soft dilution stage (first stage) is interrupted by rapid and abrupt dilution (Figure 4). This last dilution would correspond to a larger proportion of rain water; it is indistinguishable during the wet season, because rain water is mixed with water from tile drains during this period of the year (Billy et al., 2013).

In all storm events (dry and wet), for all ions (except nitrate) and EC, case 3 best simulates the third stage of the storm event (where the mixing of two end members is most evident, see Figure 4). In the second stage of the wet season storm events (Figure 4B and C), we can observe that for the chloride and sulfate ions and EC, the 3 cases have an adequate performance (although none manages to simulate the maximum dilution point, see Figure 4). In the dry season storm event (Figure 4A), the second stage of chloride and sulfate ions and EC is better simulated by case 2, followed nearby case 3; case 1 has the lowest performance of the simulations in this stage. Finally in the first stage of each of the storm events for the chloride ion, sulfate ion and EC we note the same dynamics that occurred with the second stage for case 1 and 2: case 3 performs better C_{obs} during the 2 storm events of the wet season, and case 2 performs better in the storm event of the dry season (see Figure 4A).

From this analysis we can deduce that in the dry season (Figure 4A), the first and second stages are almost completely dominated by the groundwater pool (both in terms of concentration and discharge), minimizing the other contributing pools (i.e. soil, runoff, represented by C_q and Q_q). For this reason case 2 (assuming total discharge $Q \approx Q$ groundwater) has the better performance in simulating the C_{obs} of chloride and sulfate ions in addition to EC. However, in the wet season events (Figure 4B and C), and although in the first and second stage the groundwater pool is still the main contributor, the contribution of the other pools (i.e. soil, runoff, represented by C_q and Q_q) are much more notorious. Therefore, case 3 has better performances for chloride and sulfate ions and EC.

In the case of nitrates, we must acknowledge that the combined mixing model fails to fit the observed data whatever the event (see nitrates, Figure 4). Unlike other ions, nitrates are more concentrated in soils and drain water than in groundwater or rainwater. According to Garnier et al. (2014), in the Avenelles sub-catchment, sub-root nitrate concentrations average 22 mgN.L^{-1}, close to the average concentration observed in drains in the same area (26 mgN.L^{-1}). Nitrate concentrations in the Brie aquifer are only around 13.2 mgN.L^{-1}, whereas in rainfall they are about 0.75 mgN.L^{-1} (Mouchel et al., 2016; Floury et al., 2018). For nitrate ions, a third component representing soil water would be needed as well as an appropriate parameterization of the seasonal nature of fertilizer applications. Several studies (Burns et al., 2019; Sebestyen et al., 2014) have demonstrated that for nitrate ion, more than two different concentration pools (i.e. groundwater, soil water, etc.) are involved in rising and declining limbs of hydrograph.

Table 7: Values obtained for standardized RMSE ($sRMSE$) and $bias$ for each case and solute, for an application of the combined model on selected storm events. Note that case 1 corresponds to chemostatic components, case 2 to the single 2S-APS relationship and case 3 to general case of the combined model.

Solute	Case	Short flood event, dry season (Figure 4 A)		Short flood event, wet season (Figure 4 B)		Long flood event, wet season (Figure 4 C)	
		$sRMSE$ %	$bias$ %	$sRMSE$ %	$bias$ %	$sRMSE$ %	$bias$ %
Sulfate	1	16.2	-19.0	16.9	22.0	32.3	37.7
	2	10.3	10.1	6.2	9.8	3.7	1.7
	3	7.9	-3.0	4.4	3.6	3.1	-0.5
Nitrate	1	13.1	10.1	37.9	45.6	58.8	64.4
	2	20.3	18.2	36.8	43.8	36.2	41.3
	3	21.2	16.5	34.4	9.4	40.2	-34.2
Chloride	1	28.4	-33.9	11.3	-8.9	16.3	13.8
	2	5.7	3.9	5.7	-7.1	7.0	-6.0
	3	6.4	-5.8	5.6	-6.2	4.9	1.3
EC	1	13.2	-15.0	8.7	8.6	16.3	16.9
	2	8.2	8.3	7.1	8.2	5.3	1.4
	3	4.2	-2.5	4.2	1.6	3.9	-1.1

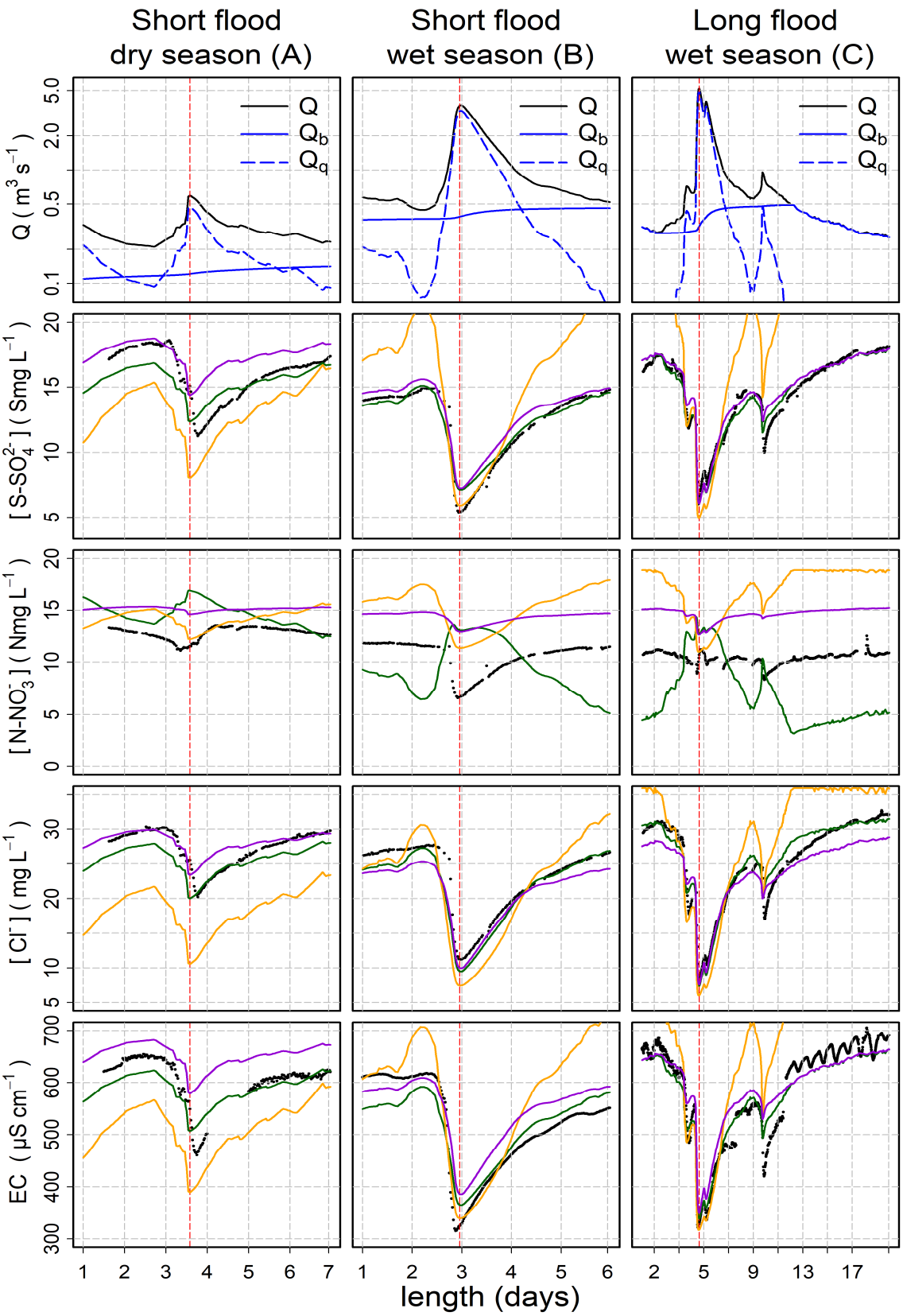

Figure 4: For the three selected storm events (short flood events during the dry season (November 2015) (A) and wet season (February 2016) (B) and long flood event (March 2016) (C)), as a function of time (days): the flow and the hydrograph separation; the comparison for solutes and EC of observed (black line) and simulated concentrations from the Case 1 (orange line), the Case 2 (violet line) and the Case 3 (green line) of the combined model.

5. Conclusions

5.1. Synthesis

The new concentration-discharge model presented in this paper associates a *classical* concentration-discharge relationship with a *classical* two-component mixing equation. The originality of our approach lies in the fact that we do not proceed in the usual way by assuming a source concentration value to perform the baseflow-quickflow separation: we use the inverse approach, and use an *a priori* assumption of the baseflow-quickflow separation to infer the source concentration values.

Our approach allows a better estimation of streamflow ionic concentration series for most ions at inter-annual scale, except for nitrate (which do not exhibit a clear $C - Q$ relationship), with improved $bias$ and $sRMSE$ criteria. This shows the advantage of coupling a time dynamic hydrological model with static $C - Q$ relations for each of the flow components.

5.2. Limits of our approach

The first limit of our approach is apparent for the nitrate case: nitrate are known to be poorly described by concentration-discharge relationships, and our model does not allow improving much the issue. The two-member hydrograph separation tested here may be a limiting factor: for nitrate ions, the two components hydrograph separation (C_q and C_b) seems to be inadequate, while for sulfate, chloride and EC, it seems sufficient. The base flow separation method used in this article carries naturally its share of uncertainties due to the arbitrary and speculative hypotheses used in its conception (Beven, 1991; Brutsaert, 2008; Cheng et al., 2016) . The "simple" separation into two components cannot explain the complexity of the behavior of the nitrate ions. Indeed, several studies (Miller et al., 2017; Probst, 1985) have shown that the introduction of a third component (which would come to represent the soil pool component) is a prerequisite to represent the behavior of nitrate.

We also need to underline that we acknowledge that our approach remains conceptual, and we do not claim to have identified ‘physically’ the water masses that produce the quick and base flow.

5.3. Further perspectives

As the model does not simulate the decoupling of discharge and concentration patterns, due to a short time lag explained by hydraulic mechanisms; doing so, would be an interesting extension of this work. An isotope study would be helpful to this aim.

Another priority would be to test the implementation of our model elsewhere, especially on high-frequency water quality stations (Kirchner et al., 2004). Different types of chemical signatures, reflecting different types of hydrological and hydro-chemical functions underlying the transfer

processes, could be studied in detail, including different flow decomposition concepts and may be other $C - Q$ relations possibly including specific seasonal features.

Another alternative would be to test this new methodology with other hydrograph separation methods than the RDF Lyne-Hollick to prove their validity (e.g. the methods developed by Eckhardt, 2005; Pelletier and Andréassian, 2020).

If high-frequency measurements become more and more available for science (Kirchner et al., 2004), their implementation at large scale still difficult and low frequencies measurements (i.e. daily, weekly) remain the rule (Moatar et al., 2017). Thus, it remains important to continue methodological development through modelling which allow us, with a limited number of measurements and a good representativeness, to assess the quality of rivers in large scale, in the framework of low frequency monitoring. Ultimately, further developments of the combined mixing model should go in this direction.

6. Acknowledgements

The first author acknowledges the Peruvian Scholarship Cienciactiva of CONCYTEC (grant no. 099-2016-

FONDECYT-DE) for supporting his PhD study at INRAE and the Sorbonne University. The authors acknowledge the EQUIPEX CRITEX program (grant no. ANR-11-EQPX-0011) for the data availability.

7. References

Ameli, A.A. et al., 2017. Primary weathering rates, water transit times, and concentration-discharge relations: A theoretical analysis for the critical zone. Water Resources Research, 53(1): 942-960. DOI:10.1002/2016wr019448

Bao, C., Li, L., Shi, Y., Duffy, C., 2017. Understanding watershed hydrogeochemistry: 1. Development of RT-Flux-PIHM. Water Resources Research, 53(3): 2328-2345. DOI:10.1002/2016wr018934

Barco, J., Hogue, T.S., Curto, V., Rademacher, L., 2008. Linking hydrology and stream geochemistry in urban fringe watersheds. Journal of Hydrology, 360(1): 31-47. DOI:https://doi.org/10.1016/j.jhydrol.2008.07.011

Barthold, F.K. et al., 2011. How many tracers do we need for end member mixing analysis (EMMA)? A sensitivity analysis. Water Resources Research, 47(8). DOI:10.1029/2011wr010604

Basu, N.B. et al., 2010. Nutrient loads exported from managed catchments reveal emergent biogeochemical stationarity. Geophysical Research Letters, 37(23).

Beven, K., 1991. Hydrograph separation?, Proceedings of the 3rd National Hydrology Symposium, Institute of hydrology, Southampton, UK, pp. 3.2-3.8.

526 Bieroza, M.Z., Heathwaite, A.L., Bechmann, M., Kyllmar, K., Jordan, P., 2018. The concentration-
527 discharge slope as a tool for water quality management. Science of The Total Environment,
528 630: 738-749. DOI:https://doi.org/10.1016/j.scitotenv.2018.02.256

529 Billy, C. et al., 2013. Factors controlling nitrate concentrations in surface waters of an artificially
530 drained agricultural watershed. Landscape Ecology, 28(4): 665-684. DOI:10.1007/s10980-
531 013-9872-2

532 Botter, M., Burlando, P., Fatichi, S., 2019. Anthropogenic and catchment characteristic signatures in
533 the water quality of Swiss rivers: a quantitative assessment. Hydrol. Earth Syst. Sci., 23(4):
534 1885-1904. DOI:10.5194/hess-23-1885-2019

535 Bouchez, J. et al., 2017. River Mixing in the Amazon as a Driver of Concentration-Discharge
536 Relationships. Water Resources Research, 53(11): 8660-8685. DOI:10.1002/2017wr020591

537 Brodie, R., Sundaram, B., Tottenham, R., Hostetler, S., Ransley, T., 2007. An overview of tools for
538 assessing groundwater-surface water connectivity. Bureau of Rural Sciences, Canberra,
539 Australia: 57-70.

540 Brutsaert, W., 2008. Long-term groundwater storage trends estimated from streamflow records:
541 Climatic perspective. Water Resources Research, 44(2).

542 Burns, D.A. et al., 2019. Monitoring the riverine pulse: Applying high-frequency nitrate data to
543 advance integrative understanding of biogeochemical and hydrological processes. Wiley
544 Interdisciplinary Reviews: Water, 6(4): e1348. DOI:10.1002/wat2.1348

545 Clow, D.W., Mast, M.A., 2010. Mechanisms for chemostatic behavior in catchments: Implications for
546 CO2 consumption by mineral weathering. Chemical Geology, 269(1): 40-51.
547 DOI:https://doi.org/10.1016/j.chemgeo.2009.09.014

548 Chanat, J.G., Rice, K.C., Hornberger, G.M., 2002. Consistency of patterns in concentration-discharge
549 plots. Water Resources Research, 38(8): 22-1-22-10. DOI:10.1029/2001wr000971

550 Chapman, T.G., 1991. Comment on “Evaluation of automated techniques for base flow and recession
551 analyses” by R. J. Nathan and T. A. McMahon. Water Resources Research, 27(7): 1783-1784.

552 Cheng, L., Zhang, L., Brutsaert, W., 2016. Automated selection of pure base flows from regular daily
553 streamflow data: objective algorithm. Journal of Hydrologic Engineering, 21(11): 1-7.

554 Durum, W.H., 1953. Relationship of the mineral constituents in solution to stream flow, Saline River
555 near Russell, Kansas. Eos, Transactions American Geophysical Union, 34(3): 435-442.
556 DOI:10.1029/TR034i003p00435

557 Eckhardt, K., 2005. How to construct recursive digital filters for baseflow separation. Hydrological
558 Processes, 19(2): 507-515.

559 Eckhardt, K., 2008. A comparison of baseflow indices, which were calculated with seven different
560 baseflow separation methods. Journal of Hydrology, 352(1-2): 168-173.

561 Evans, C., Davies, T.D., 1998. Causes of concentration/discharge hysteresis and its potential as a tool
562 for analysis of episode hydrochemistry. Water Resources Research, 34(1): 129-137.

563 Floury, P. et al., 2017. The potamochemical symphony: new progress in the high-frequency
564 acquisition of stream chemical data. Hydrol. Earth Syst. Sci., 21(12): 6153-6165.

565 Floury, P. et al., 2018. Chemical weathering and CO2 consumption rate in a multilayered-aquifer
566 dominated watershed under intensive farming: The Orgeval Critical Zone Observatory,
567 France. Hydrological Processes: 1-19.

568 Garnier, J. et al., 2016. Reconnecting crop and cattle farming to reduce nitrogen losses to river water
569 of an intensive agricultural catchment (Seine basin, France): past, present and future.
570 Environmental Science & Policy, 63: 76-90.

571 Garnier, J. et al., 2014. Curative vs. preventive management of nitrogen transfers in rural areas:
572 Lessons from the case of the Orgeval watershed (Seine River basin, France). Journal of
573 Environmental Management, 144: 125-134.

574 Godsey, S.E., Kirchner, J.W., Clow, D.W., 2009. Concentration-discharge relationships reflect
575 chemostatic characteristics of US catchments. Hydrological Processes, 23(13): 1844-1864.
576 DOI:10.1002/hyp.7315

577 Hall, F.R., 1970. Dissolved solids-discharge relationships .1. Mixing models. Water Resources
578 Research, 6(3): 845-850. DOI:10.1029/WR006i003p00845

579 Hem, J.D., 1948. Fluctuations in concentration of dissolved solids of some southwestern streams. Eos,
580 Transactions American Geophysical Union, 29(1): 80-84. DOI:10.1029/TR029i001p00080

581 Hubert, P., Martin, E., Meybeck, M., Oliver, P., Siwertz, E., 1969. Aspects hydrologique, géochimique
582 et sédimentologique de la crue exceptionelle de la Dranse du Chablais du 22 sept. 1968.
583 Arch. Sci. Soc. Phys. (Genève), 22(3): 581-603.

584 Ibarra, D.E. et al., 2016. Differential weathering of basaltic and granitic catchments from
585 concentration–discharge relationships. Geochimica et Cosmochimica Acta, 190: 265-293.
586 DOI:https://doi.org/10.1016/j.gca.2016.07.006

587 Johnson, N.M., Likens, G.E., Bormann, F.H., Fisher, D.W., Pierce, R.S., 1969. A working model for
588 variation in stream water chemistry at Hubbard-Brook-experimental-forest, new-hampshire.
589 Water Resources Research, 5(6): 1353-&. DOI:10.1029/WR005i006p01353

590 Jones, C.S., Wang, B., Schilling, K.E., Chan, K.-s., 2017. Nitrate transport and supply limitations
591 quantified using high-frequency stream monitoring and turning point analysis. Journal of
592 Hydrology, 549: 581-591. DOI:https://doi.org/10.1016/j.jhydrol.2017.04.041

593 Kirchner, J.W., 2019. Quantifying new water fractions and transit time distributions using ensemble
594 hydrograph separation: theory and benchmark tests. Hydrology & Earth System Sciences,
595 23(1).

596 Kirchner, J.W., Feng, X., Neal, C., Robson, A.J., 2004. The fine structure of water-quality dynamics: the
597 (high-frequency) wave of the future. Hydrological Processes, 18(7): 1353-1359.

598 Klemeš, V., 1986. Dilettantism in hydrology: Transition or destiny? Water Resources Research, 22(9S):
599 177-188.

600 Knapp, J.L.A., von Freyberg, J., Studer, B., Kiewiet, L., Kirchner, J.W., 2020. Concentration–discharge
601 relationships vary among hydrological events, reflecting differences in event characteristics.
602 Hydrol. Earth Syst. Sci., 24(5): 2561-2576. DOI:10.5194/hess-24-2561-2020

603 Ladson, A., Brown, R., Neal, B., Nathan, R., 2013. A standard approach to baseflow separation using
604 the Lyne and Hollick filter. Australasian Journal of Water Resources, 17(1): 25-34.

605 Longobardi, A., Loon, A.F.V., 2018. Assessing baseflow index vulnerability to variation in dry spell
606 length for a range of catchment and climate properties. Hydrological Processes, 32(16):
607 2496-2509. DOI:10.1002/hyp.13147

608 Longobardi, A., Villani, P., Guida, D., Cuomo, A., 2016. Hydro-geo-chemical streamflow analysis as a
609 support for digital hydrograph filtering in a small, rainfall dominated, sandstone watershed.
610 Journal of Hydrology, 539: 177-187.

611 Lyne, V., Hollick, M., 1979. Stochastic time-variable rainfall-runoff modelling, Institute of Engineers
612 Australia National Conference, pp. 89-93.

613 Maher, K., 2011. The role of fluid residence time and topographic scales in determining chemical
614 fluxes from landscapes. Earth and Planetary Science Letters, 312(1): 48-58.
615 DOI:https://doi.org/10.1016/j.epsl.2011.09.040

616 Maher, K., Chamberlain, C., 2014. Hydrologic regulation of chemical weathering and the geologic
617 carbon cycle. science, 343(6178): 1502-1504.

618 Mathevet, T., Michel, C., Andreassian, V., Perrin, C., 2006. A bounded version of the Nash-Sutcliffe
619 criterion for better model assessment on large sets of basins. IAHS PUBLICATION, 307: 211.

620 Meybeck, M., Moatar, F., 2012. Daily variability of river concentrations and fluxes: indicators based
621 on the segmentation of the rating curve. Hydrological Processes, 26(8): 1188-1207.

622 Miller, M.P., Tesoriero, A.J., Hood, K., Terziotti, S., Wolock, D.M., 2017. Estimating Discharge and
623 Nonpoint Source Nitrate Loading to Streams From Three End-Member Pathways Using High-
624 Frequency Water Quality Data. Water Resources Research.

625 Minaudo, C. et al., 2019. Seasonal and event-based concentration-discharge relationships to identify
626 catchment controls on nutrient export regimes. Advances in Water Resources, 131: 103379.
627 DOI:https://doi.org/10.1016/j.advwatres.2019.103379

628 Moatar, F., Abbott, B., Minaudo, C., Curie, F., Pinay, G., 2017. Elemental properties, hydrology, and
629 biology interact to shape concentration-discharge curves for carbon, nutrients, sediment,
630 and major ions. Water Resources Research, 53(2): 1270-1287.

631 Moatar, F., Meybeck, M., 2007. Riverine fluxes of pollutants: Towards predictions of uncertainties by
632 flux duration indicators. Comptes Rendus Geoscience, 339(6): 367-382.
633 DOI:https://doi.org/10.1016/j.crte.2007.05.001

634 Mouchel, J.-M., Rocha, S., Rivière, A., Tallec, G., 2016. Caractérisation de la géochimie des interfaces
635 nappe-rivière du bassin des Avenelles. Tech. rep. PIREN Seine, France, 27 pp.

636 Mouhri, A. et al., 2013. Designing a multi-scale sampling system of stream–aquifer interfaces in a
637 sedimentary basin. Journal of Hydrology, 504: 194-206.

638 Musolff, A., Fleckenstein, J.H., Rao, P.S.C., Jawitz, J.W., 2017. Emergent archetype patterns of
639 coupled hydrologic and biogeochemical responses in catchments. Geophysical Research
640 Letters, 44(9): 4143-4151. DOI:10.1002/2017gl072630

641 Musolff, A., Schmidt, C., Selle, B., Fleckenstein, J.H., 2015. Catchment controls on solute export.
642 Advances in Water Resources, 86: 133-146. DOI:10.1016/j.advwatres.2015.09.026

643 Nash, J.E., Sutcliffe, J.V., 1970. River flow forecasting through conceptual models part I—A discussion
644 of principles. Journal of hydrology, 10(3): 282-290.

645 Nathan, R., McMahon, T., 1990. Evaluation of automated techniques for base flow and recession
646 analyses. Water Resources Research, 26(7): 1465-1473.

647 Pelletier, A., Andréassian, V., 2019. Interactive comment on "Hydrograph separation: an impartial
648 parametrization for an imperfect method". Hydrol. Earth Syst. Sci. Discuss. Hydrol. Earth Syst.
649 Sci. DOI:https://doi.org/10.5194/hess-2019-503-AC2

650 Pelletier, A., Andréassian, V., 2020. Hydrograph separation: an impartial parametrisation for an
651 imperfect method. Hydrol. Earth Syst. Sci., 24(3): 1171-1187. DOI:10.5194/hess-24-1171-
652 2020

653 Pinder, G.F., Jones, J.F., 1969. Determination of the ground-water component of peak discharge from
654 the chemistry of total runoff. Water Resources Research, 5(2): 438-445.

655 Probst, J., Bazerbachi, A., 1986. Solute and particulate transports by the upstream part of the
656 Garonne river. Sciences Géologiques Bulletin: 79-98.

657 Probst, J.L., 1985. Nitrogen and Phosphorus exportation in the Garonne basin (France). Journal of
658 Hydrology, 76(3-4): 281-305. DOI:10.1016/0022-1694(85)90138-6

659 Rose, L.A., Karwan, D.L., Godsey, S.E., 2018. Concentration–discharge relationships describe solute
660 and sediment mobilization, reaction, and transport at event and longer timescales.
661 Hydrological Processes, 32(18): 2829-2844. DOI:10.1002/hyp.13235

662 Salmon, C.D., Walter, M.T., Hedin, L.O., Brown, M.G., 2001. Hydrological controls on chemical export
663 from an undisturbed old-growth Chilean forest. Journal of Hydrology, 253(1): 69-80.
664 DOI:https://doi.org/10.1016/S0022-1694(01)00447-4

665 Saraiva Okello, A.M.L. et al., 2018. Hydrograph separation using tracers and digital filters to quantify
666 runoff components in a semi-arid mesoscale catchment. Hydrological Processes, 32(10):
667 1334-1350.

668 Sebestyen, S.D., Shanley, J.B., Boyer, E.W., Kendall, C., Doctor, D.H., 2014. Coupled hydrological and
669 biogeochemical processes controlling variability of nitrogen species in streamflow during
670 autumn in an upland forest. Water Resources Research, 50(2): 1569-1591.
671 DOI:10.1002/2013wr013670

672 Stewart, M., Cimino, J., Ross, M., 2007. Calibration of base flow separation methods with streamflow
673 conductivity. Groundwater, 45(1): 17-27.

674 Tallec, G., Ansard, P., Guérin, A., Delaigue, O., Blanchouin, A., 2015. Observatoire Oracle [Data set].
675 DOI:https://dx.doi.org/10.17180/obs.oracle

Tallec, G. et al., 2013. Introduction. In: Loumagne, C., Tallec, G. (Eds.), L'observation long terme en environnement, exemple du bassin versant de l'Orgeval QUAE, Versailles, pp. 11-33.

Thompson, S., Basu, N., Lascurain, J., Aubeneau, A., Rao, P., 2011. Relative dominance of hydrologic versus biogeochemical factors on solute export across impact gradients. Water Resources Research, 47(10).

Tunqui Neira, J.M., Andréassian, V., Tallec, G., Mouchel, J.M., 2020. Technical note: A two-sided affine power scaling relationship to represent the concentration–discharge relationship. Hydrol. Earth Syst. Sci., 24(4): 1823-1830. DOI:10.5194/hess-24-1823-2020

Vaughan, M.C.H. et al., 2017. High-frequency dissolved organic carbon and nitrate measurements reveal differences in storm hysteresis and loading in relation to land cover and seasonality. Water Resources Research, 53(7): 5345-5363. DOI:10.1002/2017WR020491

Zhang, J., Zhang, Y., Song, J., Cheng, L., 2017. Evaluating relative merits of four baseflow separation methods in Eastern Australia. Journal of Hydrology, 549: 252-263.

Zhang, Q., Harman, C.J., Ball, W.P., 2016. An improved method for interpretation of riverine concentration-discharge relationships indicates long-term shifts in reservoir sediment trapping. Geophysical Research Letters, 43(19): 10215-10224. DOI:10.1002/2016gl069945

Zhang, R., Li, Q., Chow, T.L., Li, S., Danielescu, S., 2013. Baseflow separation in a small watershed in New Brunswick, Canada, using a recursive digital filter calibrated with the conductivity mass balance method. Hydrological Processes, 27(18): 2659-2665.

Zhi, W. et al., 2019. Distinct Source Water Chemistry Shapes Contrasting Concentration-Discharge Patterns. Water Resources Research, 55(5): 4233-4251. DOI:10.1029/2018wr024257